Evidence for Nb^{2+} and Ta^{3+} in silicate melts under highly reducing conditions: a XANES study

Camille CARTIER [a], Tahar HAMMOUDA [a*], Maud BOYET [a], Olivier MATHON [b], Denis TESTEMALE [cd], Bertrand N. MOINE [e] .

[a] Laboratoire Magmas et Volcans, Université Blaise Pascal - CNRS - IRD, OPGC, 5 rue Kessler, 63038 Clermont-Ferrand. (+33) 473 346775

[b] ESRF European Synchrotron Radiation Facility, 71 avenue des Martyrs, 38000 Grenoble, France. (+33) 476 882561

[c] Inst Neel, Dept MCMF, 25 avenue des Martyrs, 38042 Grenoble, France. (+33) 476 881045.

[d] ESRF, FAME Beamline, ESRF, 71 avenue des Martyrs, F-38043 Grenoble, France

[e] Laboratoire Magmas et Volcans, UMR CNRS 6524, Université Jean Monnet, 23 rue du Dr P. Michelon, F42023 SAINT-ETIENNE, CEDEX 02, France. (+33) 477 481513

* corresponding author : t.hammouda@opgc.univ-bpclermont.fr

ABSTRACT

Niobium (Nb) K-edge and tantalum (Ta) L_{III}-edge XANES spectra were acquired at the ppm (part per million) concentration level in silicate glasses quenched from chondritic melts equilibrated at 5 GPa and under moderately to highly reducing conditions (IW-1, IW-4.5, IW-7.9). Standard materials have also been analyzed for Nb and Ta, and the data were used to construct the calibration curves of E_0 (threshold energy) versus valence. Under moderately reducing conditions our results are consistent with niobium and tantalum being mainly pentavalent in the silicate melts as also suggested by previous studies. We do not exclude that at IW-1, a small fraction of Nb and Ta could be reduced, leading to a mean formal valence slightly lower than five. At IW-4.5, Ta is mainly in the form Ta^{3+}, and at IW-7.9, Ta appears to be Ta^{1+} whereas Nb is divalent (Nb^{2+}). The possibility for Nb and Ta to be present in reduced forms has implications for the behavior of the two elements during the processes of differentiation on planetary bodies formed in the reduced parts of the early solar system. Element partitioning is a function of size and valence, and our results show that high field strength elements could be reduced, which could change their chemical affinity. This may also be important for the Earth and Moon formation and early differentiation, as exemplified by the "Nb-paradox".

Keywords: Niobium – tantalum – XANES – Reduction – Silicate glass – Nb paradox

41

42 # INTRODUCTION

43 Niobium and Tantalum have been classified as High Field Strength Elements (HFSE),
44 because their ionic charge over ionic radius ratio is high. This electronic feature mostly defines
45 Nb and Ta behavior in magmatic systems: as their sizes differ significantly from that of the
46 available lattices in most of the common minerals, both elements tend to partition into the melt
47 phase during melting. Moreover Nb and Ta are described as "geochemical twins": they are
48 known to occur only in pentavalent state and octahedrally coordinated (VI-fold) in geological
49 systems, and share the same ionic radius (0.64 Å, Shannon, 1976). For those reasons, Nb and Ta
50 should behave similarly during the extraction of the core, which is the major differentiation
51 process affecting young terrestrial planets. However, the Nb/Ta ratio of the bulk silicate Earth
52 (BSE) is significantly lower than the chondritic value, unlike as expected (Mc Donough, 1991;
53 Münker et al., 2003; Rudnick et al., 2000). This observation is described as the "Niobium
54 paradox". Recently, Cartier et al. (2014a) demonstrated that this geochemical contradiction could
55 be explained by the fact that Nb and Ta can be reduced at very low oxygen fugacity (fO_2). This
56 changes the dependence of their metal-silicate partition coefficients on fO_2, causing Nb/Ta
57 fractionation relative to starting bulk chondritic value. Therefore, Nb and Ta behavior
58 (partitioning) in metal-silicate systems is mainly controlled by oxygen fugacity (fO_2).

59 There are several ways to estimate cation oxidation states in magmatic systems. Metal-silicate
60 melt partition coefficients as a function of fO_2 diagrams can be used to infer cation formal valence
61 in the silicate melt. Such data are consistent with Nb being pentavalent (Nb^{5+}) in moderately
62 reducing conditions ($fO_2 >$ IW- 3, i.e. above 3 log units below Iron – Wustite buffer) and divalent
63 (Nb^{2+}) in reducing conditions ($fO_2 <$ IW- 4), whereas Ta is pentavalent (Ta^{5+}) in moderately

reducing conditions (fO_2 > IW-2) and trivalent (Ta^{3+}) in reducing conditions (fO_2 < IW-4, Cartier et al., 2014a). Furthermore, the behavior of ions in crystal-melt systems is in part governed by how effortlessly they substitute for other ions in crystal lattices, and that this substitution is mainly controlled by the ionic radius and the ionic charge of the element (Brice, 1975; Wood and Blundy, 1997).

X-ray absorption near edge structure (XANES) spectroscopy can be an effective tool to study element's oxidation states. For example, Burnham et al. (2012) found that at oxygen fugacity between IW-4.3 and IW+6.7 and pressures from ambient to 1.5 GPa, Nb and Ta occur exclusively as Nb^{5+} and Ta^{5+}. At present, Nb and Ta oxidation states under more reducing conditions have only been inferred from partitioning behavior as a function of fO_2. The aim of the present study is to determine directly valence states at conditions relevant to early planetary body evolution, i.e. highly reducing conditions. For this purpose, we equilibrated metal-silicate systems at 5 GPa and under various redox conditions (IW-1, IW-4.5 and IW-7.9), and then probed Nb and Ta environments in quenched silicate melts using XANES technique.

EXPERIMENTAL

Experiments have been performed in multi-anvil apparatus at 5 GPa with variable oxygen fugacitiy at Laboratoire Magmas et Volcans (Clermont-Ferrand, France). The fO_2 was imposed by adding different amounts of metallic Si to the starting powders modifying the metal/oxide ratio of the sample. All experiments were performed using graphite capsules. The fO_2 values of the experimental charges have been determined following the thermodynamical formalism based on the Si-coesite equilibrium and fully described in Cartier et al. (2014b). In brief, we used the

$$SiO_2 = Si + O_2$$

equilibrium, wherein SiO_2 is coesite and Si is alloyed to Fe. The activity of Si in solution in the metallic alloy was determined using its concentration determined by electron microprobe, and the activity coefficient provided by the "metal activity calculator" of the Oxford petrology group. The activity of SiO_2 is 1 because coesite is present in the experiments. Finally, we write

$$fO_2 = \exp\left(-\frac{\Delta G^\circ}{RT}\right) \cdot \left(\frac{a_{SiO_2}}{a_{Si}^{alloy}}\right),$$

with ΔG° the standard free-energy change, T the temperature of the experiment and R the gas constant.

Three different starting materials were used. Samples #1198 and #1207 were investigated in the study of Cartier et al. (2014,a) who also conducted experiments on Nb and Ta partitioning as a function of fO_2 and proposed valence state for the two elements. Sample #1198 is a tholeiitic basalt doped with 200 ppm Nb and Ta and mixed with Fe metal and S. Sample #1207 consists of EL6 meteorite powder doped with 200 ppm Nb and Ta and mixed with 2 wt.% Si metal. Sample #1243 was synthetized for the present study and consists of EL6 meteorite material doped with

3200 ppm Nb and Ta and mixed with 42 wt.% Si metal (Table 1). All starting materials were doped with Nb and Ta as AAS standard solutions.

Experimental charges were mounted in epoxy, ground and polished. The samples comprised metallic quenched melt, silicate quenched melt (glass), enstatite, coesite and sulfide melt in variable proportions. Chemical compositions have been analyzed using an electron microprobe CAMECA SX100 and an Agilent 7500-cs induced coupled plasma – mass spectrometer (ICP-MS) coupled with a Resonetics M-50 laser at the LMV (Clermont-Ferrand).

X-RAY ABSORPTION SPECTROSCOPY

Setup

Nb K edge and Ta L_{III} edge XANES data were acquired at the X-ray absorption spectroscopy (XAS) beamline BM23 of the European Synchrotron Radiation Facility (ESRF in Grenoble, France). Measurements were performed using a Si(111) double crystal monochromator coupled to a micro-XAS station. This station is based on a set of Pt coated mirrors in a Kirkpatrick-Baez (KB) geometry and a sample area specially designed for XAS measurements. The incident angle of the two mirrors could be varied from 2 to 8 mrad allowing XAS operation up to 40 keV with a maximum numerical aperture. The optical arrangement of the KB mirrors allows obtaining a focal spot of 4 by 4 mm^2. The stability of the beam during a XAS energy scan is below 1 mm/keV in both transverse directions. The micro-XAS sample area part is based on a double mechanical stage mounted in series. The first stage is designed to align the sample environment part on the X-ray beam after the double reflection on the KB mirrors. The second stage, based on a commercial hexapod, allows scanning the sample into the X-ray beam. The micro-XAS station

is equipped with mini ionization chambers developed in-house and a Vortex solid-state fluorescence detector. The setup is completed with a visible microscope with variable magnification.

Energy calibration

Given the need for thermal stability of the monochromator during the long time periods needed for an experiment, and the necessary precision needed on E_0 values to derive redox data, following procedure was established in order to model the monochromator drift. Figure 1 displays the threshold energies E_0 of Nb-foils measured during a week of beam time, and plotted as a function of time. One recalibration is visible after ~35h. The energy shift was parameterized as a polynomial function of time (intervals B and C) to correct every spectra acquired during the week from the drift.

Data acquisition and processing

For Nb, standard material was prepared in the form of pellets consisting of mixture of BN with NbO, NbO_2 and Nb_2O_5, for Nb^{2+}, $Nb^{4+}$and Nb^{5+} references, respectively. We also used an Nb foil, as a reference for Nb^0. In the same way, pellets made of mixture of Ta_2O_5 and BN were used as Ta^{5+} reference, and a Ta foil was used as Ta^0 reference. We also used $GaTa_4Se_8$, which contains a mixture of Ta^{4+} and Ta^{3+} in equal amounts, resulting in a mean formal valence of 3.5. However the latter was only used for the quantitative valence versus E_0 (threshold energies) calibration (see later), and not for comparing the sample and reference XANES spectra because the Ta speciation in $GaTa_4Se_8$ is too different from the oxide structure. The niobium oxide

powders were purchased from Alfa Aesar and ground to 1-10 μm. The XANES data on oxide-BN pellets and metallic foils were acquired in transmission mode, and $GaTa_4Se_8$ was measured in fluorescence mode. All sample data (1198, 1207 and 1243) were collected in fluorescence mode, using the Vortex solid-state detector.

The experimental samples contain metal blobs immersed in the silicate melt. In order to avoid XANES signal contamination by metal fluorescence, we first acquired XRF maps of element distribution determined with the electron microprobe analysis of all the samples were used to select homogeneous and metal-free areas, as shown in Figure 2.

Because of the very low Nb and Ta concentrations of experimental samples (see Table 2), many spectra were accumulated for each experimental sample. These were subsequently stacked, thus improving counting statistics. Moreover, for each experimental sample, XANES data acquired on different points were used in order to check for potential contamination (from metal blobs) and heterogeneities in the melt. For both reference and sample XANES spectra, the different XANES analysis steps (inspection of individual spectra, merging, correction of E_0 and normalization) were performed with the ATHENA software from the Horae package (reference Ravel and Newville, 2005), based on the Ifeffit library (Newville, 2001). We defined the threshold energy E_0 as the first significant peak of the derivative (selecting the zero-crossing of the 2^{nd} derivative curve with Athena software).

RESULTS

All details on the experimental conditions are given in Table 1. This study focuses on the silicate melt, of which the chemical compositions are given in Table 2. Table 3 summarizes the number of spectra that have been merged to produce the data presented below, together with the acquisition time for individual spectra. The data were obtained using a total acquisition time between 5.5 and 15 hours. We checked that spectra did not change during the acquisition period. Nb contents are comprised between 2.5 and 313 ppm, and Ta is in the range 21.9 – 282.7 ppm. At reducing conditions, Nb and Ta are siderophile and enter preferentially the metal phase (Cartier et al., 2014a). As a consequence the Nb and Ta concentration of quenched silicate melt of 1207 and 1243 are quite low (Nb: 8.4 and 2.5 ppm respectively; Ta: 201.5 and 21.9 ppm respectively, see Table 2). Nb oxidation state in experiment 1207 was not determined in this study.

As the region near the X-ray-absorption edge is scanned in energy, the ejected photoelectron sequentially probes the empty electronic levels of the material (Wong et al., 1984). XANES is strongly sensitive to the chemistry of the absorbing atom and various XANES spectral features can be interpreted in terms of local symmetry of the absorbing atom (Mottana, 2004). Pre-edge features of the X-ray-absorption edge spectra are caused by electronic transitions to empty bound states and give information on the oxidation state of the atom and local bonding characteristics (coordination). Finally the post-edge features of the XANES spectra are dominated by multiple-scattering resonance of the photoelectrons ejected at low energy. These features can be correlated with the atomic positions of the neighboring atoms. The present study is focused on the determination of Nb and Ta formal valence in various conditions. Thus we combined two methods. For the first approach, we compared qualitatively our samples spectra to reference spectra to find similarities (shape and edge position). In a second approach, we established a calibration curve for the edge position (E_0) versus formal oxidation state of the reference

compounds to determine the valence of our experimental samples. Most of the times, the chemical shifts (edge position) vary linearly with the valence of the atom, a phenomenon known as Kunzl's law (Kunzl, 1932). In this study, we applied a calibration curve based on oxides compounds to quenched glasses. As discussed below, this should have little effect on the conclusions.

Niobium

Nb K-edge XANES spectra and corresponding first derivatives are shown on Figure 3. The four reference samples (standards) look similar to those obtained in previous studies (Burnham et al., 2012; Froideval et al., 2008). Niobium threshold energy E_0 is shifted from 18986 eV (Nb^0) to 19006 eV (Nb^{5+}) as Nb formal valence increases. As already noticed by Froideval et al. (2008), the white line intensity of the reference samples is also affected by Nb oxidation state, as well as the shape of the spectra. In Nb_2O_5, NbO_2 and NbO, Nb is octahedrally (and more or less distorted) coordinated, mainly due to the large radius of the element (Jehng and Wachs, 1990; Nico et al., 2011). Piilonen et al. (2006) showed that for Nb^{5+}, site distortion could result in shifting of E_0 position. For the purpose of the present investigation, the potential consequences of this shift are limited, and will be addressed below.

From all the spectra (samples and references) presented on Figure 3, we defined the threshold energy E_0 as the first significant peak of the derivative (selecting the zero-crossing of the 2nd derivative curve with Athena software). The results are given in Table 4 and are plotted on Figure 4. The reference samples were used to calibrate the dotted line. In order to evaluate the uncertainty associated to valence determination, we adopted the following approach. First we

211 determined the error on E_0 determination. Taking into account the beamline resolution, the
212 approximation of taking E_0 as the first derivative peak on noisy spectra, the variability between
213 the spectra that results in a deviation on the merged spectra, and the error associated to the
214 normalization procedure, we estimate the global uncertainty on E_0 to be approximately ± 0.5 eV.
215 Due to the large energy shift between Nb and Nb^{5+} (20 eV), the corresponding error on Nb
216 valence is then ~ 0.1. As shown by Piilonen et al. (2006) in the case of Nb^{5+}, site distortion can
217 shift the E_0 value by 2.6 eV at most. Taken this additional uncertainty yields error on Nb valence
218 state of approximately ~ 0.6.

219 Sample #1198, the oxygen fugacity of which is IW-1, is similar to Nb_2O_5 (Fig.3),
220 especially in pre-peak and edge features. When plotted on the valence calibration curve, Nb mean
221 valence of #1198 has been found to be 4.4 ± 0.6 at IW-1. We conclude here that in this sample,
222 Nb is mainly 5+ and is octahedrally coordinated. This result is consistent with previous studies
223 that argue for Nb to remain pentavalent in silicate systems and between IW+7 and IW-4.2.

224 Sample #1243, with an oxygen fugacity of IW-7.9, looks similar to NbO. The oscillations
225 (the first three low intensity peaks) in the pre-edge part of the derivative are mainly related to the
226 noise on #1243 Nb spectra and have not to be taken into account (the Nb concentration is indeed
227 very low at ~2ppm, Table 1). However the shoulder on the pre-edge position is not exactly the
228 same for #1243 and NbO. In the same way the depression in the XANES region is very similar
229 for the two spectra but seems to be shifted on the low energies for #1243. This should indicate
230 that in this sample, Nb is mainly 2+, and its coordination is octahedral, although the surrounding
231 atoms may not be only oxygen (O^{2-}) but also sulfur (S^{2-}) (see melt composition in Table 2). The
232 calibration curve gives a mean valence of 1.9 ± 0.6, in agreement with the qualitative
233 observations.

Tantalum

Ta LIII-edge XANES spectra and corresponding first derivatives are shown on Figure 5. The two reference samples are plotted on Figure 5 with the three experimental samples for comparison. From Ta^0 to Ta^{5+}, Ta E_0 shifts from 9881 to 9882.8 eV. This shift is relatively small (1.8 eV instead of 20 eV for Nb), and as consequence, the error associated to the determination of the valence is significantly high (1.3) compared to that of Nb (0.1), even though we estimate the error on E_0 determination to be the same than Nb (± 0.5 eV).

Qualitatively, spectra of #1198 and #1207 are quite similar to that of Ta_2O_5, but seem to be slightly shifted toward the low energies. Likewise, the white line is split into two components peaks for both samples, unlike Ta_2O_5. This feature has already been observed by Burnham et al. (2012) and Farges et al. (2006). The white line in #1243 spectrum is located between those of Ta-foil and sample 1207. This indicates Ta formal valence in #1243 is less than 5.

For the valence versus E_0 calibration line, the same procedure as for Nb is employed here. Ta threshold energies have been defined as the first significant peaks of the derivatives for experimental samples and references. Results are given in Table 5 and displayed on Figure 6. The E_0 values of the standards define a linear calibration line with a good correlation. When plotted on this line, samples display the following mean valences for Ta: +4.6 ± 1.3 at IW-1, +3.1 ± 1.3 at IW-4.5, and +0.7 ± 1.3 at IW-7.9.

DISCUSSION

The results of the XANES measurements are summarized in Figure 7. Here, it should be noted that crystalline reference compounds were applied to the study of experimental glasses. As noted by Piilonen et al. (2006) in the case of Nb, the E_0 value depends on the crystalline structure and site symmetry around Nb, even for constant valence state. Therefore, the calibration curve obtained in the present study may be slightly affected. We note however that in the case of Nb, the shift due to crystallographic structure is about 2.5 eV (Piilonen et al., 2006), which is low relative to the total shift due to valence change from Nb° to Nb^{5+}. Moreover, the position of the white line is constant for the metal. Therefore, the uncertainty on valence determination arises solely from the position of the charged Nb ion edge energy. This difference is small compared to the observed shift among the samples studied, making the conclusion on Nb valence change robust. For the Ta case, it is known that the L-edge is due to the excitation of 2p electrons to d-state (Burnham et al., 2012) and the corresponding energy is usually less sensitive to the atom environment.

Although the number of data points is limited, the trend for both Nb and Ta is unambiguous: reducing oxygen fugacity from IW-1 to IW-7.9 yields valence reduction for both Nb and Ta. For the moderately reducing conditions (IW-1), Nb and Ta are predominantly in the 5+ state. The present study is compatible with Burnham et al., (2012) who found that, between IW+6.7 and IW-4.3, niobium and tantalum are mainly pentavalent in silicate melts. For more reducing conditions (IW-4.5), Ta becomes trivalent. This finding is contradictory with Burnham et al. (2012) who conclude that Ta is pentavalent down to IW-4.3, but agrees with the interpretation of the oxygen fugacity dependent trace element partitioning results reported in Cartier et al. (2014b) as shown in Figure 7. The discrepancy between our results and those of Burnham et al. (2012) could be due to the fact that we used an E_0 vs. valence calibration curve, whereas Burnham et al.

only compared qualitatively the XANES spectra of samples equilibrated under various fO_2. We do not exclude that it could also be due to differences in melt compositions, but we note that both glasses equilibrated at ca. IW-4 have comparable SiO_2 concentrations and that their structure, expressed as the number of non-bridging oxygens per tetrahedrally-coordinated cations (NBO/T ratio, Mysen, 1987) are close (0.37 in our case vs. 0.25 in Burnham et al. (2012)).

At IW-7.9, Nb becomes divalent, whereas Ta is further reduced, maybe down to about 1+. The Ta results should be considered with caution because of the large error on mean valence determination. Nevertheless, as shown in Figure 7, our results are in good agreement with Cartier et al. (2014a) Nb and Ta valence estimation from experimentally determined metal – silicate partition coefficient versus oxygen fugacity relationship.

It is not clear from Figure 7 whether there is a crossover in the valence states of Nb and Ta. The data suggest that Ta is reduced to a formal valence of ca. +1 or less, which implies a crossover. However, Cartier et al. (2014a) found that the metal silicate partition coefficients of Nb and Ta merge at very low fO_2. This finding may imply that both elements have the same valence state at very reducing conditions. The low count number using the Ta L_{III} edge combined with the small shift of Ta white line position across the range of valence states yields high uncertainties on valence state determination. Finally, both Nb and Ta become highly siderophile at very low fO_2 (Cartier et al., 2014a), which yields extremely low concentrations in the silicate melt for both elements. Low concentration is an additional difficulty when attempting to directly determine Nb and Ta valence state. Our approach, which consists of combining experimental geochemistry (using information from partition coefficients, Cartier et al., 2014a) with spectroscopic methods, appears to be a good tradeoff for valence determination at extreme conditions (pressure, temperature, oxygen fugacity) such as explored in the present study.

IMPLICATIONS

For elements whose valence varies across the range of the solar system oxygen fugacity values (IW-6 or less in enstatite chondrites to IW+8 in oxidized Earth's rocks (Wadhwa, 2008; Larimer and Buseck, 1974)), it can be anticipated that their affinity with host minerals would change, depending on ambient conditions (Papike et al., 2005). Such may be the case for Nb and Ta.

Recently, the Nb paradox (that is, the Nb deficit in the bulk silicate Earth relative too Ta) has been re-evaluated in terms of the effect oxygen fugacity on metal – silicate partitioning during the Earth's core segregation (Cartier et al., 2014a). Moreover, very recent studies report on anomalous Nb behavior in supposedly undifferentiated extraterrestrial material. Barrat et al. (2014) measured Nb negative anomalies in EL and EH5 enstatite chondrite silicate parts. Varela et al. (2014) discovered correlation between V and Nb depletions in chondrule cores of enstatite chondrite. These concentrations could be linked to the equilibration and/or removal of a metallic or sulphide phase occurring during the history of these objects, under conditions wherein Nb is siderophile and / or chalcophile. The latter behavior would be analogous to that of Ti, another HFSE, which was demonstrated as being chalcophile and divalent in Yamato 691 enstatite chondrite (Nakamaru-Messenger et al., 2012). Here, we have calibrated the valence of Nb and Ta in silicate melts as a function of fO_2. Although Nb and Ta concentrations in natural melts are very low, and consequently acquiring XANES spectra would be challenging, obtaining direct information on those element valence in solar system primitive objects could help in evaluating the oxygen fugacity that they recorded.

ACKNOWLEDGEMENTS

We gratefully acknowledge Anthony Burnham and Laurent Cario (Institut des Matériaux Jean Rouxel, Nantes) for providing us with reference material. We also thank the ESRF FAME team for the training course. We gratefully acknowledge comments and helpful suggestions by N. Bennett and an anonymous reviewer, as well as additional comments by editor B. Mysen. This work was supported by the European Synchrotron Radiation Facility (proposal ES-122). This research received funding from the European Research Council under the European Community's Seventh Framework Program (FP7/2007-2013 Grant Agreement 209035) and from the French PNP program (INSU-CNRS). The multianvil apparatus of Laboratoire Magmas et Volcans is financially supported by the Centre National de la Recherche Scientifique (Instrument National de l'INSU). This research was partly supported by the French Government Laboratory of Excellence initiative ANR-10-LABX-0006, the Région Auvergne, and the European Regional Development Fund. This is Laboratory of Excellence *ClerVolc* contribution № 142.

REFERENCES

Barrat J.A., Zanda B., Jambon A., and Bollinger C. (2014) The lithophile trace elements in enstatite chondrites. Geochimica et Cosmochimica Acta, 128, 71–94.

Brice J.C. (1975) Some thermodynamic aspects of the growth of strained crystals. Journal of Crystal Growth, 28, 249–253.

Burnham A.D., Berry A.J., Wood B.J. and Cibin G. (2012) The oxidation states of niobium and tantalum in mantle melts. Chemical Geology, 330-331, 228–232.

Cartier C., Hammouda T., Boyet M., Bouhifd M.A. and Devidal J.-L. (2014a). Redox control of the fractionation of niobium and tantalum during planetary accretion and core formation. Nature Geoscience, 7, 573–576.

Cartier C., Hammouda, T., Doucelance R., Boyet M., Devidal J.L. and Moine B. (2014b). Experimental study of trace element partitioning between enstatite and melt in enstatite chondrites at low oxygen fugacities and 5GPa. Geochimica et Cosmochimica Acta, 130, 167–187.

Farges F., Linnen R.L., and Brown G.E. (2006) Redox and speciation of tin in hydrous silicate glasses: a comparison with Nb, Ta, Mo AND W. The Canadian Mineralogist, 44, 795–810.

Froideval A., Degueldre C., Segre C.U., Pouchon M., and Grolimund D. (2008) Niobium speciation at the metal/oxide interface of corroded niobium-doped Zircaloys: A X-ray absorption near-edge structure study. Corrosion Science, 50, 1313–1320.

Jehng J.M., and Wachs I. E. (1990). The molecular structures and reactivity of supported niobium oxide catalysts. Catalysis Today, 8, 37–55.

Kunzl V. (1932) Collection des Travaux de Chimie de Tchécoslovaquie 4, 213-224.

Larimer J. W., and Buseck P. R. (1974). Equilibration temperatures in enstatite chondrites. Geochimica et Cosmochimica Acta, 38, 471–477.

McDonough W.F. (1991). Partial melting of subducted oceanic crust and isolation of its residual eclogitic lithology. Philosophical Transactions of the Royal Society of London A., 335, 407-418.

A. Mottana (2004) X-ray absorption spectroscopy in mineralogy: Theory and experiment in the XANES region. In Spectroscopiec Methods in Mineralogy, ed. : A. Beran & E. Libowitzky, European Mineralogical Union Notes in Mineralogy Volume 6, 465-522.

Münker C., Pfänder J.A., Weyer S., Büchl A., Kleine T., and Mezger K. (2003). Evolution of planetary cores and the Earth-Moon system from Nb/Ta systematics. Science, 301, 84–7.

Mysen B.O. (1987) Magmatic silicate melts: relation between bulk composition, structure and properties. In Magmatic Processes: Physicochemical Principles, B.O. Mysen, Editor, The Geochemical Society Special Publication No 1, 375-399.

Nakamura-Messenger K., Clemett S.J., Rubin A.E., Choi b.-G., Zhang S., Rahman Z., Oikawa K., and Keller L.P. (2012) Wassonite: A new titanium monosulfide mineral in the Yamato 691 enstatite chondrite. Amer. Mineral. 97, 807-815.

Newville M. (2001) IFEFFIT : interactive XAFS analysis and FEFF fitting. Journal of Synchrotron Radiation, 8, 322–324.

Nico C., Soares M.R.N., Rodrigues J., Matos M., Monteiro R., Graça M.P.F, and Monteiro, T. (2011). Sintered NbO Powders for Electronic Device Applications. Journal of Physical Chemistry C 115, 4879–4886.

Papike J.J., Karner J.M., and Shearer C.K. (2005). Comparative planetary mineralogy: Valence state partitioning of Cr, Fe, Ti, and V among crystallographic sites in olivine, pyroxene, and spinel from planetary basalts. American Mineralogist, 90, 277-290.

Piilonen P.C., Farges F., Linnen R.L., Brown G.E. Jr, Pawlak M. and Pratt A. (2006) Structural environment of Nb^{5+} in dry and fluid-rich (H_2O, F) silicate glasses: a combined XANES and EXAFS study. The Canadian Mineralogist 44, 775-794.

Ravel B., and Newville M. (2005) ATHENA, ARTEMIS, HEPHAESTUS: data analysis for X-ray absorption spectroscopy using IFEFFIT. Journal of Synchrotron Radiation, 12, 537–41.

Rudnick R., Barth M., Horn I., and McDonough W. (2000) Rutile-bearing refractory eclogites: missing link between continents and depleted mantle. Science, 287, 278–81.

Shannon R.D. (1976) Revised Effective Ionic Radii and Systematic Studies of Interatomie Distances in Halides and Chaleogenides. Acta Crystallographica A, 32, 751–767.

Varela M.E., Sylverster P., Brandstätter F., and Engler A. (2014) Non-porphyric chondrules in enstatite chondrites. In 77th Annual Meteoritical Society Meeting.

396 Wadhwa, M. (2008) Redox conditions on small bodies, the Moon and Mars. Reviews in
397 Mineralogy and Geochemistry, 68, 493-510.

398 Wong J., Lytle F.W., Messmer R.P., and Maylotte D.H. (1984) K-edge absorption spectra of
399 selected vanadium compounds. Physical Reviews B, 30, 5596–5610.

400 Wood B.J., and Blundy J.D., (1997) A predictive model for rare earth element partitioning
401 between clinopyroxene and anhydrous silicate melt. Contributions to Mineralogy and
402 Petrology, 129, 166–181.

403

TABLES

Table 1. Experimental conditions.

Experiment	Pressure (GPa)	Temperature (K)	Starting material	Nb2O5 doped (ppm)	Ta2O5 doped (ppm)	Metal added (wt.%)	fO_2 ΔIW
1198	5	2073	Tholeitic basalt	200	200	Fe + S	-1
1207	5	2073	EH6 chondrite	200	200	2 % Si	-4.5
1243	5	1973	EH6 chondrite	3200	3200	42 % Si	-7.9

Table 2. Electron microprobe and ICP-MS analysis of the three experimental quenched melts.

Experiment	1198		1207		1243	
Electron probe (wt.%)	*Na=4*	*1σ*	*Na=4*	*1σ*	*Na=3*	*1σ*
Si	19.22	0.15	30.55	0.25	28.22	0.15
Ti	0.40	0.04	0.09	0.05	0.01	0.01
Al	8.10	0.08	3.41	0.38	2.01	0.02
Cr	0.05	0.05	0.04	0.03	0.01	0.02
Fe	10.02	0.23	0.36	0.10	0.15	0.01
Mn	0.10	0.02	0.20	0.07	0.04	0.03
Mg	8.78	0.16	9.44	0.56	15.12	0.20
Ca	7.53	0.15	3.51	0.15	2.32	0.09
Na	1.44	0.03	1.89	0.20	1.11	0.05
K	0.04	0.03	0.53	0.10	0.18	0.01
Ni	0.01	0.01	0.02	0.03	0.02	0.02
S	0.13	0.05	0.95	0.06	7.77	0.12
O	43.06	0.09	44.71	1.33	41.43	0.15
Total	98.86		95.71		98.45	
C*	1.14		4.29		1.55	0.27
ICP-MS (ppm)	*Na=5*	*1σ*	*Na=5*	*1σ*	*Na=4*	*1σ*
Nb	312.9	11.0	8.4	4.9	2.5	0.3
Ta	282.7	12.6	201.5	11.5	21.9	0.7

*Notes :** C content is calculated by difference between 100 % and the total.
Na = number of analyses

411

412 **Table 3.** Details on data acquisition, with number of stacked spectra for each experiment,
413 together with acquisition time (in minutes) for each individual spectrum.

414

Exp. Sample	Niobium		Tantalum	
	Nb of stacked spectra	Acquisition time (minutes/spectrum)	Nb of stacked spectra	Acquisition time (minutes/spectrum)
1198	22	28	30	29
1207	no data		11	29
1243	26	24	20	29

415

416

417 **Table 4.** Nb threshold energies of references and experimental samples, and corresponding
418 valences.

419

Sample	E_0	Valence
Nb foil	18986	0
NbO	18994.7	2
NbO_2	19002.8	4
Nb_2O_5	19006.0	5
1243	18994.1	1.9 ±0.6
1198	19004.09	4.4 ±0.6

420

421

422 **Table 5.** Ta threshold energies of references and experimental samples, and corresponding
423 valences.

424

Sample	E_0	Valence
Ta foil	9881	0
$GaTa_4Se_8$	9882.1	3.5
Ta_2O_5	9882.8	5
1243	9881.2	0.7 ±1.3

1207	9882.1	3.1 ±1.3
1198	9882.6	4.6 ±1.3

FIGURE CAPTION

Figure 1. Nb-foil measurements during the week of analysis. Black dots correspond to Nb-foil measurements, which E0 has been defined as the absorption spectra first derivative peaks. Nb-foil E0 is 18986 eV. The A period corresponds to monochromator stabilization. A recalibration was done between B and C periods. All sample analyses have been done between these Nb-foils measurements and we consequently applied to every point an energy shift correction corresponding to the ΔShift on the figure. In detail, Nb spectra for sample 1198 have been acquired during the B period, and all other spectra, including experimental and reference samples, have been acquired during the C period.

Figure 2. **Combined Nb and Fe map of sample 1243**. The red part corresponds to the area with the highest Nb and Fe concentrations, i.e. an outcropping metal blob. The rounded green part is less concentrated in those elements and corresponds to a metal blob hidden beneath the surface. The blue area is Fe and Nb poor and corresponds to the quenched silicate melt. The structures (metal blebs, homogeneous melt area…) have been identified comparing the maps with SEM pictures of the samples.

Figure 3. Niobium spectra for standards and samples (left) and their derivative (right). Increase in Nb oxidation state causes an increase in E0. Sample 1198 (IW-1) is similar to Nb_2O_5 and sample 1243 is similar to NbO.

Figure 4. Niobium oxidation state versus E0 calibration. The straight line is defined by a linear regression on the four standards (black filled circles). Then, the edge energies (E0) of the samples (grey filled diamonds) have been plotted to estimate their mean valence. Sample 1198 Nb mean valence is 4.4 ± 0.1 and Sample 1243 mean valence is 1.9 ± 0.1.

Figure 5. Tantalum spectra for standards and samples (left) and their derivative (right). Increase in Ta oxidation state causes an increase in E0. Sample 1198 is similar to Ta_2O_5. Samples 1207 and 1243 are increasingly shifted on the left but the lack of standards prevent us to define the Ta prevailing configurations.

Figure 6. Tantalum oxidation state versus E0 calibration. The straight line is defined by a regression on the three standards (black filled circles). Then, the edge energies (E0) of the samples (grey filled diamonds) have been plotted to estimate their mean valence. Sample 1198 Ta mean valence is 4.6 ± 1.3, Sample 1207 Ta mean valence is 3.1 ± 1.3, and Sample 1243 Ta mean valence is 0.7± 1.3. The rather large error is due to the very small energy shifts induced by the valence changes in Ta.

Figure 7. Nb (in blue) and Ta (in red) valence states as a function of oxygen fugacity. The results obtained in the present study (symbols at given fO_2 values) agree with values deduced from experimentally determined metal – silicate partition coefficients (Cartier et al., 2014a), shown as colored boxes, and with determination at IW-5.5 from enstatite / silicate melt partition (Cartier et al., 2014b) shown as hexagon. Open boxes with dotted contours represent the results of Burnham et al. (2012). Due to analytical constraints, the presence of Ta^{1+} is uncertain, as discussed in the main text. Errors on valence state are discussed in the text. Uncertainties on oxygen fugacity (±0.5 log units) have been discussed in Cartier et al. (2014b).

Figure 1

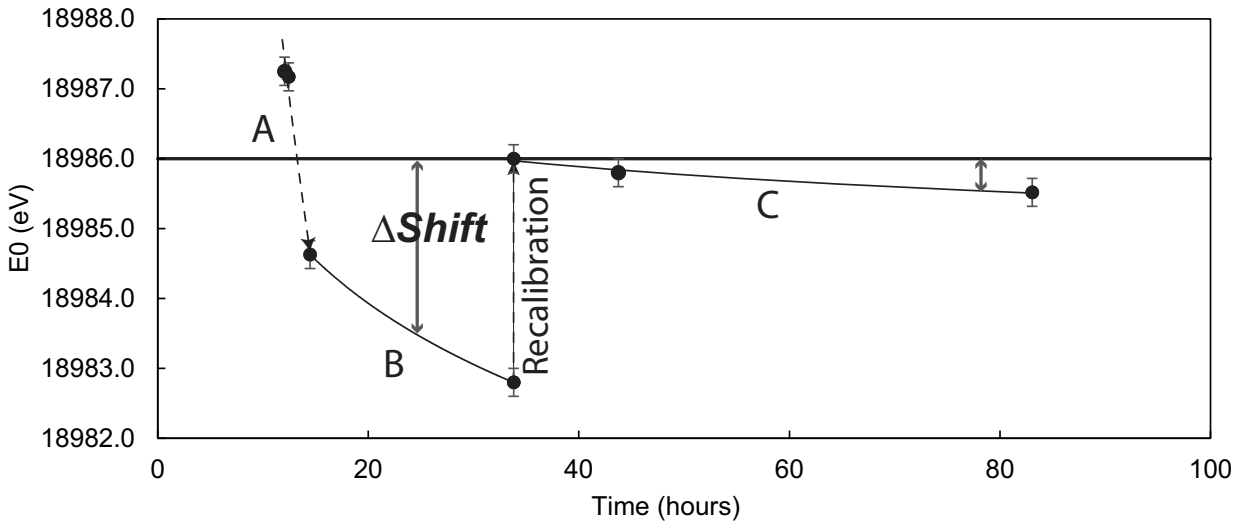
18988.0
18987.0
18986.0
18985.0
18984.0
18983.0
18982.0
E0 (eV)
0
20
40
60
80
100
Time (hours)
A
B
C
ΔShift
Recalibration

Figure 2

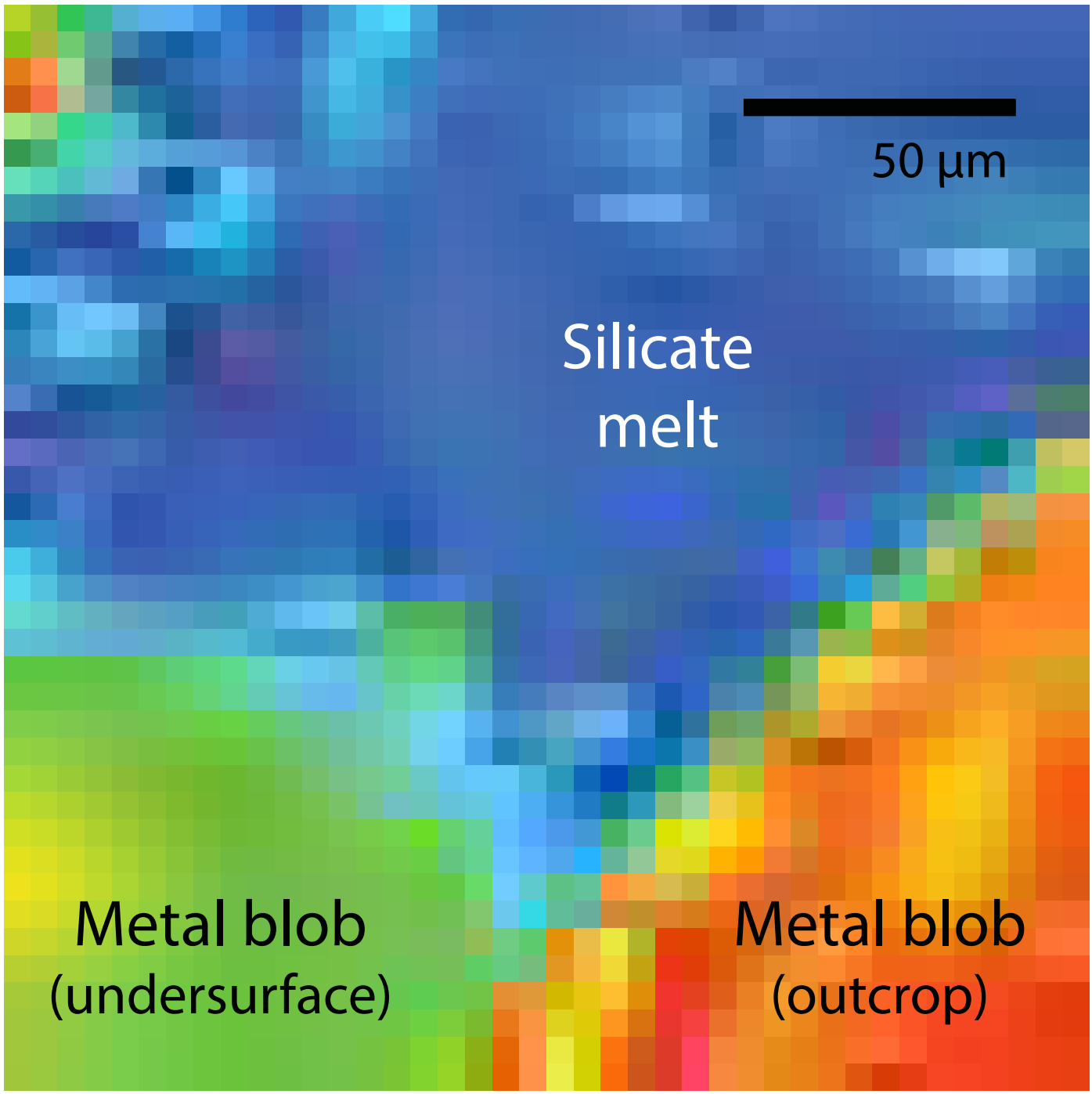
50 µm
Silicate melt
Metal blob (undersurface)
Metal blob (outcrop)

Figure 3

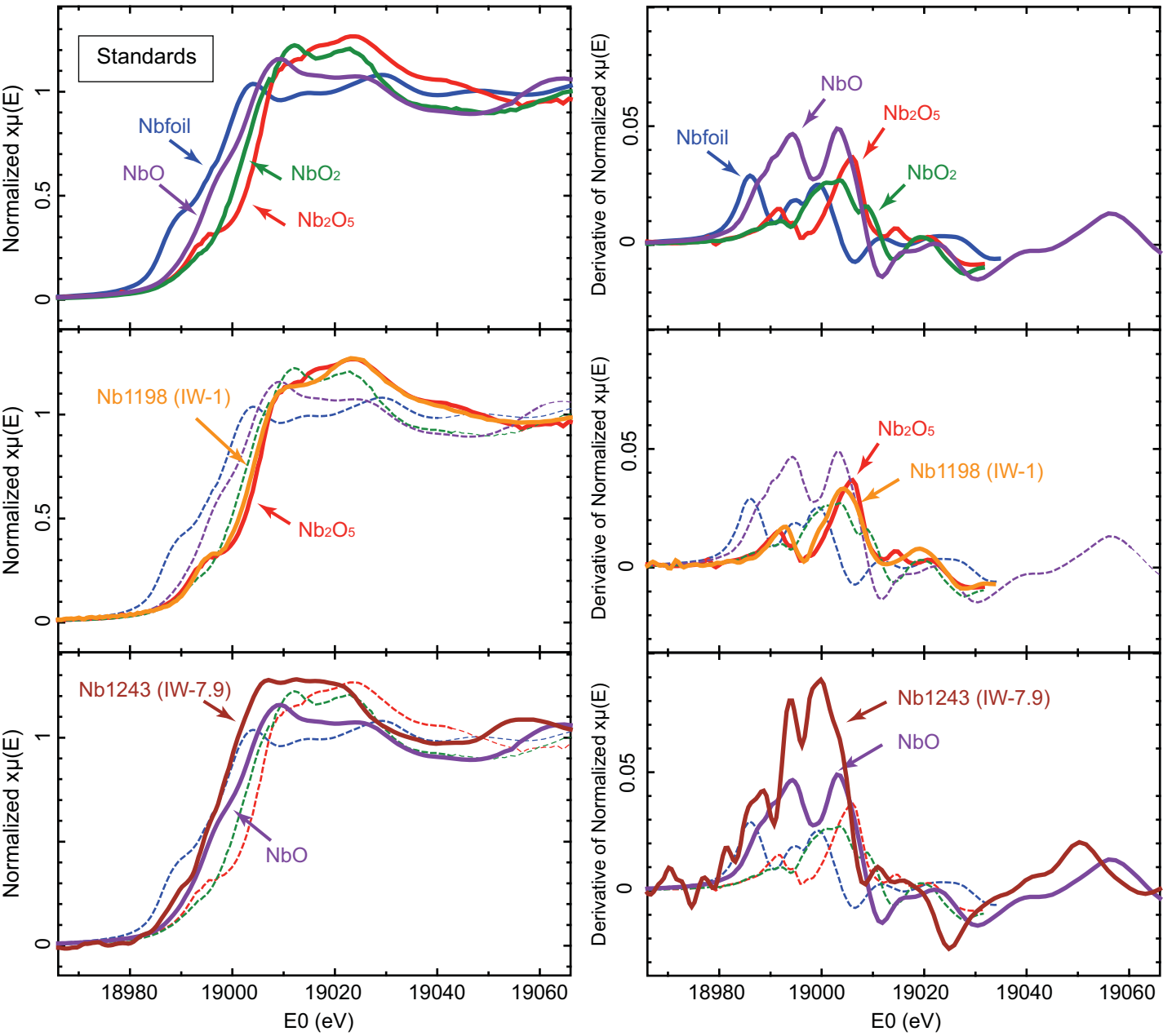
Standards
Nbfoil
NbO
NbO2
Nb2O5
Nb1198 (IW-1)
Nb2O5
Nb1243 (IW-7.9)
NbO
Normalized xμ(E)
Derivative of Normalized xμ(E)
0
0.5
1
0.05
18980
19000
19020
19040
19060
E0 (eV)

Figure 4

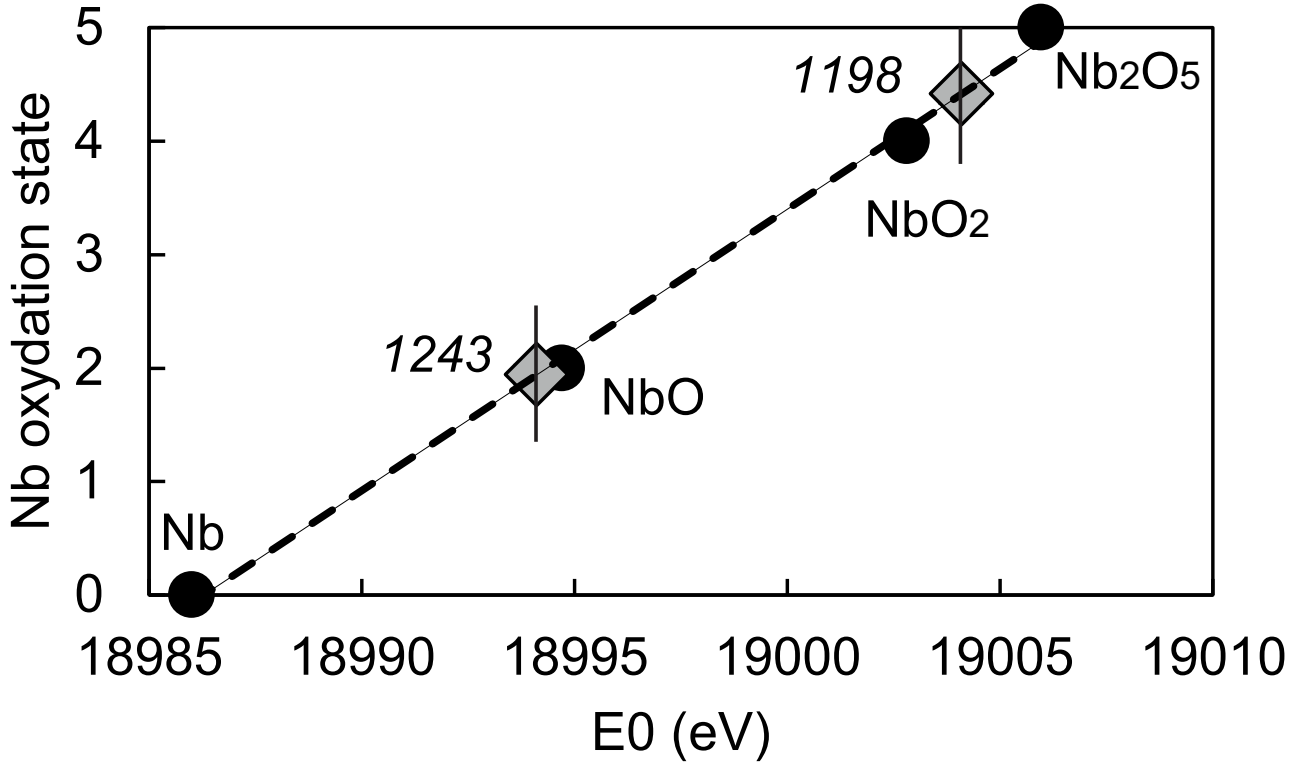
Nb oxydation state
5
4
3
2
1
0
18985
18990
18995
19000
19005
19010
E0 (eV)
Nb
1243
NbO
1198
NbO2
Nb2O5

Figure 5

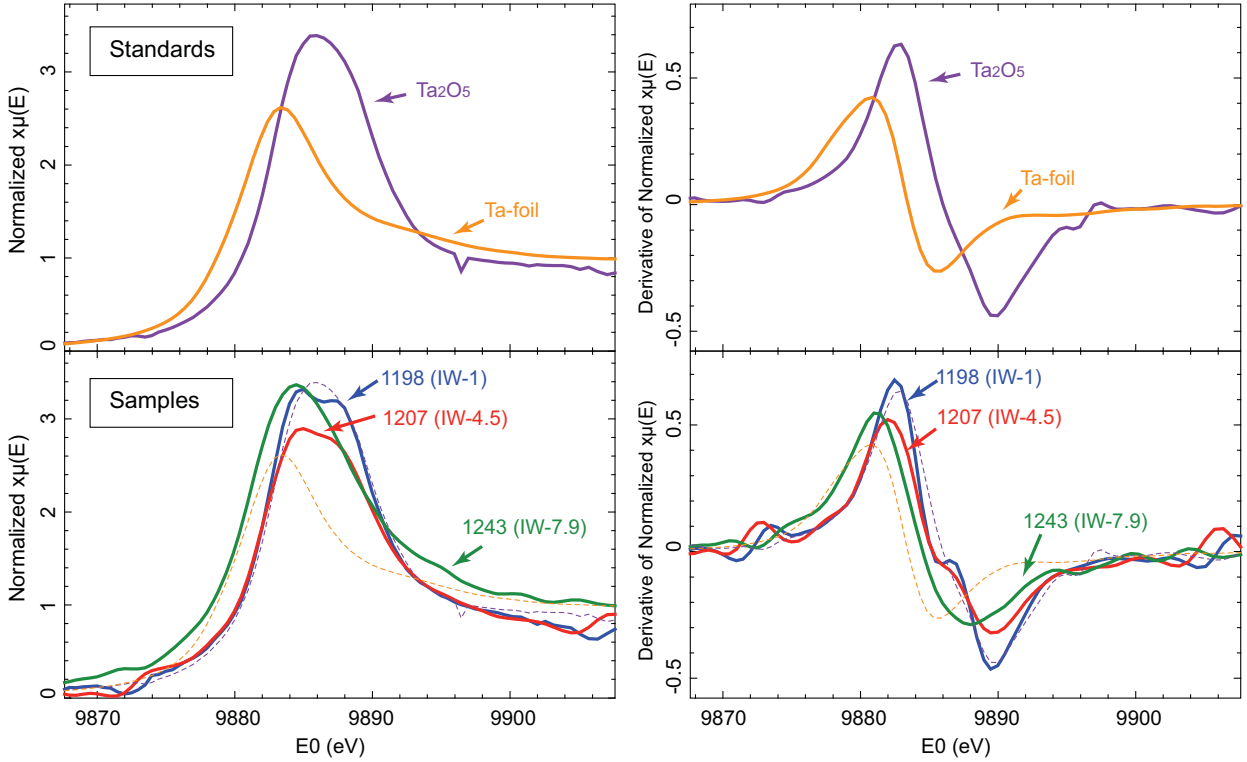
Standards
Ta2O5
Ta-foil
Normalized xμ(E)
Derivative of Normalized xμ(E)
Samples
1198 (IW-1)
1207 (IW-4.5)
1243 (IW-7.9)
E0 (eV)
9870
9880
9890
9900
0
1
2
3
-0.5
0.5

Figure 6

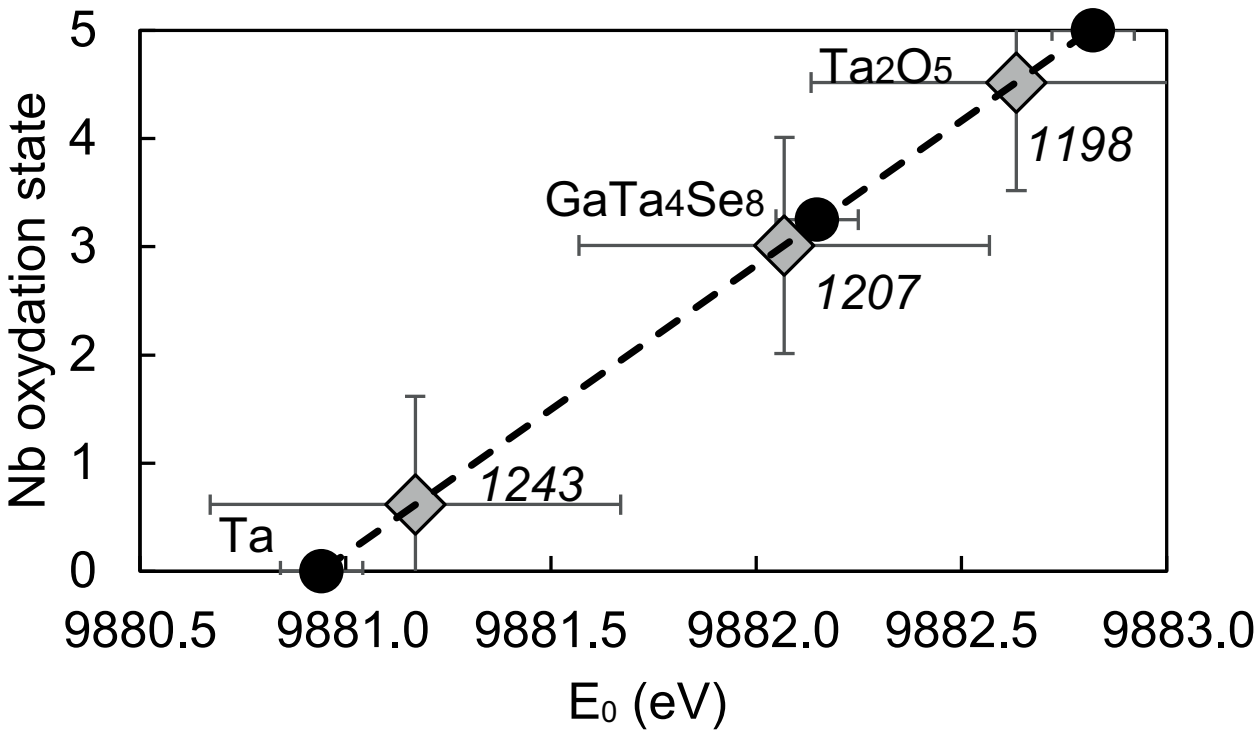
Nb oxydation state
5
4
3
2
1
0
9880.5
9881.0
9881.5
9882.0
9882.5
9883.0
E0 (eV)
Ta2O5
1198
GaTa4Se8
1207
1243
Ta

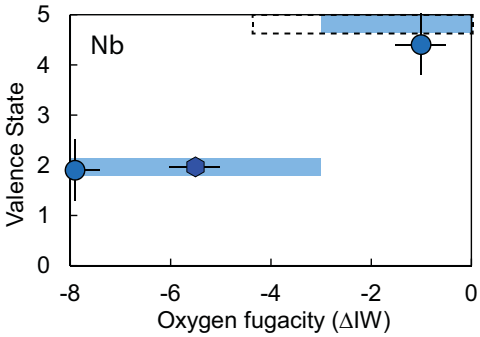
Nb
Valence State
Oxygen fugacity (ΔIW)
5
4
3
2
1
0
-8
-6
-4
-2
0

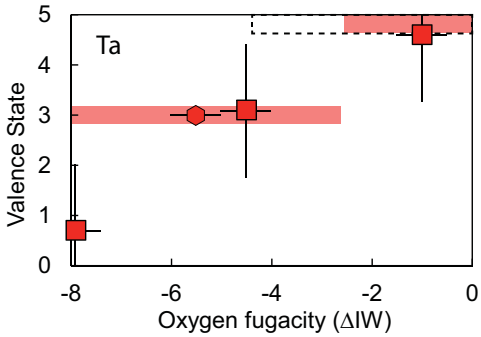
Ta
Valence State
Oxygen fugacity (ΔIW)
5
4
3
2
1
0
-8
-6
-4
-2
0

Figure 7